INTERNATIONAL JOURNAL FOR NUMERICAL METHODS IN FLUIDS, VOL. 25, 151–166 (1997)

A PSEUDOSPECTRAL CODE FOR CONVECTION WITH AN ANALYTICAL/NUMERICAL IMPLEMENTATION OF HORIZONTAL BOUNDARY CONDITIONS

S. M. COX* AND P. C. MATTHEWS

Department of Theoretical Mechanics, The University of Nottingham, University Park, Nottingham NG7 2RD, U.K.

SUMMARY

A new code for simulating convection in a horizontal layer of fluid is described. The code can be used to study the usual Rayleigh–Bénard convection problem but can also incorporate internal heating, rotation and the vortex force responsible for Langmuir circulation. Boundary conditions in the horizontal directions are periodic, but a wide range of conditions may be imposed on the upper and lower boundaries.

A novel feature of the method is the way in which these boundary conditions are implemented through the following analytical/numerical technique. The governing partial differential equations are reduced to a number of inhomogeneous second-order ODEs for the horizontal Fourier modes. The solutions to these are then written as the sum of a particular integral and a complementary function. The former is easily computed (numerically) without regard to the boundary conditions and the latter is then selected (analytically/numerically) to ensure that the boundary conditions are met.

We apply our code to the problem of highly supercritical thermal convection in a shear flow. We compare our results with simulations in the literature and, by integrating over a longer time interval, find flow features not observed in the previous simulations, including stable time-dependent states, multiple stable equilibria and chaos.

Int. J. Numer. Meth Fluids, **25**: 151–166 (1997).

No. of Figures: 5. No. of Tables: 2. No. of References: 13.

KEY WORDS: convection; shear flow; boundary conditions; pseudospectral

1. INTRODUCTION

Rayleigh–Bénard convection is a topic of intensive research. In addition to its many geophysical applications, convection is of interest as a mechanism for pattern formation and also for the transition to turbulence. Much of the research in this field is based on numerical simulations. Since a large amount of time is spent in formulating algorithms and writing codes, it is important that details of methods are published in order to avoid unnecessary duplication of effort.

Our code solves the Navier–Stokes and heat equations for convection in a horizontal layer of fluid. The formulation of the governing equations is similar to that of Lundbladh *et al.*[1] for the Navier–

* Correspondence to: S. M. Cox, Department of Theoretical Mechanics, The University of Nottingham, University Park, Nottingham NG7 2RD, U.K.

Contract grant sponsor: Nuffield Foundation
Contract grant sponsor: University of Nottingham
Contract grant sponsor: Royal Society

CCC 0271–2091/97/020151–16 $17.50 *Received May 1996*

Stokes equation only. As in their code, the non-linear terms are computed in physical space and time stepping is done in spectral space. The solution is assumed to be periodic in the two horizontal directions. However, our code allows a wide range of conditions at the horizontal boundaries, which are imposed by a novel numerical/analytical method. Mixed boundary conditions may be applied to the horizontal velocity components and the temperature at the top and bottom boundaries, where 'mixed' means that a linear combination of each physical quantity and its first vertical derivative is specified. To describe how the boundary conditions are applied, we first note that the code is pseudospectral, with functions being expanded in Fourier modes in the horizontal directions (x and y) and Chebyshev modes in the vertical (z). At each time step the governing equations are reduced to a set of ordinary differential equations (ODEs) in z for each Fourier mode of various physical quantities. However, not all these quantities have known boundary conditions and a number of the ODEs must be solved before the physical velocity components can be reconstructed and the boundary conditions applied. Our procedure is to solve the ODEs formally by writing the solution to each as the sum of a particular integral and a complementary function. The former can easily be calculated and the latter is just the sum of two exponential functions of z. The coefficients of the exponentials are unknown, but they can be carried through the calculation analytically and finally determined when the velocity boundary conditions are applied at the end of the time step.

Besides permitting generalized boundary conditions, the code allows a wide range of convection problems to be investigated. The fluid layer may be heated from below, corresponding to Rayleigh–Bénard convection. A shear flow driven by the boundary conditions on the horizontal velocity components may be imposed. This facility is of interest in atmospheric and oceanographic applications, where convection may take place in the presence of a mean wind or current. At present only plane Couette flow may be driven because no mean horizontal pressure gradient may be imposed. A rotating frame of reference may be used, with the rotation vector at any angle to the vertical. If rotation is combined with a mean flow driven by the horizontal boundaries, then convection in an Ekman layer may be examined. Internal heating may be included. Our code can also simulate Langmuir circulation, which is a wind-driven convective motion occurring naturally in oceans and lakes. To simulate Langmuir circulation using the Craik–Leibovich model,[2,3] a 'vortex force' must be introduced into the governing equations. Our code allows a comprehensive treatment of the Langmuir circulation problem since it may be examined in a rotating, stratified layer.

In Section 2 we introduce the governing equations for convection and rewrite them in a form suitable for numerical solution. The ways in which the equations are discretized in time and horizontally in space are discussed in Section 3. The mathematical procedure for solving the boundary value problems in z that result from the horizontal space discretization is summarised in Section 4, before the numerical implementation of the analysis is addressed in Section 5. We have written all the code from scratch, apart from the Fourier and Chebyshev transforms (where we have used those of Lundbladh *et al.*[1]). We have tested our code thoroughly by comparing it with analytical and other numerical results for two- and three-dimensional convection. Some of the comprehensive checks we have carried out on our code are described in Section 6. In Section 7 we present some new results for convection at large Rayleigh number in a strong shear flow, which extend calculations of Hathaway and Somerville.[4] By extending the period of integration by a factor of about 10, however, we find flow features not observed by Hathaway and Somerville.[4] We draw our conclusions in Section 8.

2. GOVERNING EQUATIONS

We consider convection in a horizontal fluid layer and begin by non-dimensionalizing the problem in the standard way.[5] If D is the depth of the fluid layer and κ is the thermal diffusivity, then we adopt

the following scales: D for lengths, D^2/κ for time, κ/D for velocity. The fluid is assumed to be incompressible and Boussinesq with reference density ρ_0, so $\rho_0\kappa^2/D^2$ serves as a scale for pressure. The scale for temperature differences is ΔT. For standard Rayleigh–Bénard convection between isothermal boundaries, ΔT is the temperature difference across the fluid layer. We make the problem dimensionless using these scales.

The flow domain is then

$$0 < x < L_x, \qquad 0 < y < L_y, \qquad -\tfrac{1}{2} < z < \tfrac{1}{2},$$

where (x, y, z) form a Cartesian co-ordinate system: x and y are the horizontal co-ordinates and z is a vertical co-ordinate increasing upwards.

The governing equations are

$$\frac{1}{\sigma}\left(\frac{\partial \mathbf{u}}{\partial t} + (\mathbf{u}\cdot\nabla)\mathbf{u} - 2\mathbf{u}\times\boldsymbol{\Omega}\right) = -\nabla p + RaT\hat{\mathbf{z}} + \nabla^2\mathbf{u} + \frac{1}{\sigma}\mathbf{U}_S\times(\boldsymbol{\omega} + 2\boldsymbol{\Omega}), \tag{1}$$

$$\frac{\partial T}{\partial t} + [(\mathbf{u} + \mathbf{U}_S)\cdot\nabla]T = \nabla^2 T + I, \tag{2}$$

$$\nabla\cdot\mathbf{u} = 0. \tag{3}$$

Here $\mathbf{u} = (u, v, w)$ is the fluid velocity, T is the temperature difference from a reference temperature T_0, p is the pressure and $\boldsymbol{\omega} = \nabla\times\mathbf{u}$ is the vorticity. The parameters appearing are the Prandtl number $\sigma = \nu/\kappa$, where the kinematic viscosity of the fluid is ν, and the Rayleigh number $Ra = \gamma g\Delta T D^3/\nu\kappa$, where g is the acceleration due to gravity and γ is the coefficient of cubical expansion, i.e. $\rho(T) = \rho_0[1 - \gamma(T - T_0)]$, where $\rho_0 = \rho(T_0)$. The unit vertical vector is denoted by $\mathbf{z}$. The dimensionless rotation vector $\boldsymbol{\Omega}$ is related to the Taylor number Ta by $Ta = 4\Omega^2/\sigma^2$, where $\Omega = |\boldsymbol{\Omega}|$. The direction $\hat{\boldsymbol{\Omega}} = \boldsymbol{\Omega}/\Omega$ of the rotation axis may be chosen in any orientation. I is the strength of internal heating, which is assumed to be constant (possibly zero).

If Langmuir circulation is to be simulated according to Craik–Leibovich theory,[2] then $\mathbf{U}_S$ is the Stokes drift; otherwise $\mathbf{U}_S$ is set to zero. For Langmuir circulation the Stokes drift will be in the x-direction, with $\mathbf{U}_S = U_S(z)\hat{\mathbf{x}}$, where $U_S(z)$ is given by

$$U_S(z) = \begin{cases} Rz & \text{if } \beta = 0 \\ (R/2\beta)\mathrm{e}^{2\beta z} & \text{if } \beta > 0. \end{cases}$$

Here β (proportional to the wave number of the surface gravity waves) determines the depth profile of the Stokes drift and

$$R = \frac{D^2}{\kappa}\frac{dU_S^{\mathrm{dim}}}{dz^{\mathrm{dim}}}\bigg|_{z=1/2}$$

determines its magnitude. The superscript 'dim' indicates that the corresponding quantity is taken prior to the non-dimensionalization process.

The code can be used to simulate thermal convection in the presence of an imposed shear flow. At present no mean horizontal pressure gradient is allowed, so it is not possible to simulate Poiseuille flow. Plane Couette flow can be driven by motion of the horizontal boundaries or by applied stresses. The time and velocity scales chosen above for the non-dimensionalization are appropriate for thermal diffusion but are not the natural choices for shear flows and shear flow instabilities (such as Langmuir circulation). It is therefore necessary for us to rescale some of our results by the Prandtl number in order to compare them with those in the literature.[6]

A useful diagnostic of the convection is the Nusselt number

$$N_+ = \int\int \frac{\partial}{\partial z} T(x, y, \tfrac{1}{2}, t)\mathrm{d}x\ \mathrm{d}y.$$

This is the ratio of the heat conducted through the upper boundary in the presence of convection to that in the absence of convection (in which case the heat transfer is purely by conduction). A similar Nusselt number N_- characterizes the heat transport through the lower boundary.

2.1. Reduction of governing equations

We now reduce the vector equation (1) to a pair of scalar equations, for the vertical component of the vorticity, ω_3, and the Laplacian of the vertical velocity component w,[7] using the equation of continuity (3). This is the approach adopted by Lundbladh *et al.*[1]

We begin by using the vector identity $\mathbf{u} \times \boldsymbol{\omega} = \frac{1}{2}\boldsymbol{\nabla}|\mathbf{u}|^2 - (\mathbf{u}\cdot\boldsymbol{\nabla})\mathbf{u}$ to rewrite (1) as

$$\frac{1}{\sigma}\left(\frac{\partial \mathbf{u}}{\partial t} + \tfrac{1}{2}\boldsymbol{\nabla}|\mathbf{u}|^2 - \mathbf{u} \times (\boldsymbol{\omega} + 2\boldsymbol{\Omega})\right) = -\boldsymbol{\nabla} p + RaT\hat{\mathbf{z}} + \nabla^2\mathbf{u} + \frac{1}{\sigma}\mathbf{U}_\mathrm{S} \times (\boldsymbol{\omega} + 2\boldsymbol{\Omega}). \tag{4}$$

We then introduce $\mathbf{H} = \mathbf{u} \times (\boldsymbol{\omega} + 2\boldsymbol{\Omega})$ and take the curl of (4) to eliminate the pressure and give the vorticity equation

$$\frac{1}{\sigma}\left(\frac{\partial \boldsymbol{\omega}}{\partial t} - \boldsymbol{\nabla} \times \mathbf{H}\right) = Ra\frac{\partial T}{\partial y}\hat{\mathbf{x}} - Ra\frac{\partial T}{\partial x}\hat{\mathbf{y}} + \nabla^2\boldsymbol{\omega} + \frac{1}{\sigma}\left((\omega_3 + 2\Omega_3)U_\mathrm{S}'\hat{\mathbf{x}} - U_\mathrm{S}\frac{\partial \boldsymbol{\omega}}{\partial x}\right). \tag{5}$$

The z-component of (5) provides us with a scalar equation for ω_3:

$$\frac{\partial \omega_3}{\partial t} = \frac{\partial H_2}{\partial x} - \frac{\partial H_1}{\partial y} + \sigma\nabla^2\omega_3 - U_\mathrm{S}\frac{\partial \omega_3}{\partial x}. \tag{6}$$

If we now take the curl of (5), we find

$$\frac{\partial \nabla^2\mathbf{u}}{\partial t} = \nabla^2\mathbf{H} - \boldsymbol{\nabla}(\boldsymbol{\nabla}\cdot\mathbf{H}) + \sigma Ra\nabla^2 T\hat{\mathbf{z}} - \sigma Ra\frac{\partial}{\partial z}\boldsymbol{\nabla}T + \sigma\nabla^4\mathbf{u} - \boldsymbol{\nabla} \times \left(\omega_3 U_\mathrm{S}'\hat{\mathbf{x}} - U_\mathrm{S}\frac{\partial \boldsymbol{\omega}}{\partial x}\right).$$

The z-component of this equation provides a scalar equation for w:

$$\frac{\partial \nabla^2 w}{\partial t} = \nabla_\mathrm{H}^2 H_3 - \frac{\partial}{\partial z}\left(\frac{\partial H_1}{\partial x} + \frac{\partial H_2}{\partial y}\right) + \sigma Ra\nabla_\mathrm{H}^2 T + \sigma\nabla^4 w + U_\mathrm{S}'\frac{\partial \omega_3}{\partial y} - U_\mathrm{S}\nabla^2\frac{\partial w}{\partial x}. \tag{7}$$

The notation ∇_H^2 is used for the horizontal Laplacian.

With this procedure the pressure has been eliminated and there remain the three scalar equations (2), (6) and (7) to be solved.

2.2. Boundary conditions

All physical quantities are periodic in x and y since we shall represent them in terms of discrete Fourier modes and so no action need be taken to impose periodic lateral boundary conditions.

The following boundary conditions apply to the velocity components: at $z = \frac{1}{2}$,

$$\alpha_1\frac{\partial u}{\partial z} + \alpha_2 u = U_\mathrm{top}, \qquad \alpha_5\frac{\partial v}{\partial z} + \alpha_6 v = V_\mathrm{top}, \qquad w = 0, \tag{8}$$

and at $z = -\frac{1}{2}$,

$$\alpha_3 \frac{\partial u}{\partial z} + \alpha_4 u = U_{\text{btm}}, \qquad \alpha_7 \frac{\partial v}{\partial z} + \alpha_8 v = V_{\text{btm}}, \qquad w = 0, \tag{9}$$

where U_{top}, U_{btm}, V_{top} and V_{btm} are constants. These boundary conditions cover a wide variety of cases. For example, if we set $\alpha_1 = \alpha_3 = \alpha_5 = \alpha_7 = 0$, $\alpha_2 = \alpha_4 = \alpha_6 = \alpha_8 = 1$ and $U_{\text{top}} = U_{\text{btm}} = V_{\text{top}} = V_{\text{btm}} = 0$, these are the conditions for stationary rigid boundaries. Alternatively, a constant horizontal velocity of the boundaries may be imposed, to drive a mean shear flow, or a constant stress may be applied, for example. Mixed boundary conditions are particularly useful for the problem of Langmuir circulation.[8]

The temperature satisfies

$$\alpha_9 \frac{\partial T}{\partial z} + \alpha_{10} T = T_{\text{top}} \quad \text{at } z = \tfrac{1}{2}, \qquad \alpha_{11} \frac{\partial T}{\partial z} + \alpha_{12} T = T_{\text{btm}} \quad \text{at } z = -\tfrac{1}{2}. \tag{10}$$

A common assumption is that the horizontal boundaries are isothermal and this circumstance can be achieved, for example, by setting $\alpha_9 = \alpha_{11} = 0$, $\alpha_{10} = \alpha_{12} = 1$ and T_{top} and T_{btm} to the temperatures on the top and bottom boundaries respectively. Of course, isothermal boundaries are a mathematical idealization in which the boundary material conducts heat infinitely better than the fluid. When the conductivities of the fluid and the boundary material are comparable, the problem of heat transport in the fluid should be solved together with the corresponding heat conduction problem in the boundaries. For simplicity, however, we avoid this approach and instead model the general boundary conditions on the temperature by the 'Newton law of cooling' given in (10). General values for α_9–α_{12} are supposed to simulate finitely conducting horizontal boundaries.

2.3. Mathematical problem

The modified governing equations (2), (6) and (7) can be written in the form

$$\frac{\partial \phi}{\partial t} = h_\phi + \sigma \nabla^2 \phi, \tag{11}$$

$$\nabla^2 w = \phi, \tag{12}$$

$$\frac{\partial \omega_3}{\partial t} = h_\omega + \sigma \nabla^2 \omega_3, \tag{13}$$

$$\frac{\partial T}{\partial t} = h_T + \nabla^2 T. \tag{14}$$

Here we have introduced $\phi = \nabla^2 w$ and the hs are given by

$$h_\phi = \nabla_{\text{H}}^2 H_3 - \frac{\partial}{\partial z}\left(\frac{\partial H_1}{\partial x} + \frac{\partial H_2}{\partial y}\right) + \sigma Ra \nabla_{\text{H}}^2 T + U_{\text{S}}' \frac{\partial \omega_3}{\partial y} - U_{\text{S}} \nabla^2 \frac{\partial w}{\partial x},$$

$$h_\omega = \frac{\partial H_2}{\partial x} - \frac{\partial H_1}{\partial y} - U_{\text{S}} \frac{\partial \omega_3}{\partial x}, \qquad h_T = -[(\mathbf{u} + \mathbf{U}_{\text{S}}) \cdot \boldsymbol{\nabla}]T + I.$$

Once w and ω_3 have been found, u and v can be reconstructed from the definition of ω_3 and the continuity equation, which yield

$$\nabla_{\text{H}}^2 u = -\frac{\partial^2 w}{\partial x \partial z} - \frac{\partial \omega_3}{\partial y}, \qquad \nabla_{\text{H}}^2 v = -\frac{\partial^2 w}{\partial y \partial z} + \frac{\partial \omega_3}{\partial x}. \tag{15}$$

The horizontal means of u and v, denoted $\bar{u}$ and $\bar{v}$, cannot be calculated from such expressions and for these we return to the horizontally averaged Navier–Stokes equations:

$$\frac{\partial \bar{u}}{\partial t} = \overline{H_1} + \sigma D^2 \bar{u}, \qquad \frac{\partial \bar{v}}{\partial t} = \overline{H_2} + \sigma D^2 \bar{v} - U_S \Omega_3, \tag{16}$$

where $D = \partial/\partial z$.

3. DISCRETIZATION

3.1. Horizontal space discretization

A truncated Fourier series is used to discretize in the horizontal directions so that

$$u = \sum_{n_x=-N_x}^{N_x} \sum_{n_y=-N_y}^{N_y} \hat{u}(n_x, n_y) \exp[\mathrm{i}(n_x k_x x + n_y k_y y)],$$

for example, where

$$k_x = \frac{2\pi}{L_x}, \qquad k_y = \frac{2\pi}{L_y}.$$

The transformed variable $\hat{u}(n_x, n_y)$ is a function of z and t only. Because the solution is real-valued, the programme considers explicitly only $0 \leqslant n_y \leqslant N_y$, with the negative-$n_y$ modes obtained as complex conjugates of the positive-n_y modes.

For the (n_x, n_y) mode the exact equations to be satisfied are, from (11)–(14),

$$\frac{\partial \hat{\phi}}{\partial t} = \hat{h}_\phi + \sigma(D^2 - k^2)\hat{\phi}, \tag{17}$$

$$(D^2 - k^2)\hat{w} = \hat{\phi}, \tag{18}$$

$$\frac{\partial \hat{\omega}_3}{\partial t} = \hat{h}_\omega + \sigma(D^2 - k^2)\hat{\omega}_3, \tag{19}$$

$$\frac{\partial \hat{T}}{\partial t} = \hat{h}_T + (D^2 - k^2)\hat{T}, \tag{20}$$

where $k^2 = n_x^2 k_x^2 + n_y^2 k_y^2$. The 'hatted' variables are the Fourier transforms of the corresponding 'unhatted' variables.

The discretization in z will be discussed in Section 5.

3.2. Time discretization

We turn now to the time discretization. We use explicit, Adams–Bashforth time stepping for the non-linear terms (except for an initial Euler step when the solution is available only at the initial time) and the implicit trapezium rule for the linear terms. For an equation of the form

$$\frac{\partial f}{\partial t} = Lf + N(f),$$

where L represents the linear diffusion terms and N the $\hat{h}$s in (17)–(20), our time stepping gives

$$f^{n+1} = f^n + \frac{\Delta t}{2}(Lf^{n+1} + Lf^n) + a_n N(f^n) + b_n N(f^{n-1}),$$

where Δt is the (constant) time step. The superscript indicates the time step at which the solution is evaluated. The coefficients (a_n, b_n) are chosen to be $(\Delta t, 0)$ for an initial Euler time step (when only the current function values are known) and $(\frac{3}{2}\Delta t, -\frac{1}{2}\Delta t)$ otherwise for an Adams–Bashforth time step. This equation may be rewritten as

$$\left(1 - \frac{\Delta t}{2}L\right)f^{n+1} = \left(1 + \frac{\Delta t}{2}L\right)f^n + a_n N(f^n) + b_n N(f^{n-1}).$$

We need to recast (17)–(20) in time-discretized form. All four discretizations are similar (even that for $\hat{w}$). For $\phi(n_x, n_y)$ the discretized equation is

$$\left(1 - \frac{\Delta t\sigma}{2}(D^2 - k^2)\right)\hat{\phi}^{n+1} = \left(1 + \frac{\Delta t\sigma}{2}(D^2 - k^2)\right)\hat{\phi}^n + a_n\hat{h}_\phi^n + b_n\hat{h}_\phi^{n-1}.$$

This is an inhomogeneous, second-order, constant coefficient ODE for $\hat{\phi}^{n+1}$. A rearrangement of the terms gives

$$(D^2 - \lambda^2)\hat{\phi}^{n+1} = \hat{f}_\phi^n, \tag{21}$$

where

$$\lambda^2 = k^2 + \frac{2}{\Delta t\sigma},$$
$$\hat{f}_\phi^n = -(D^2 - \lambda^2)\hat{\phi}^n - \frac{4}{\Delta t\sigma}\hat{\phi}^n - \frac{2}{\Delta t\sigma}(a_n\hat{h}_\phi^n + b_n\hat{h}_\phi^{n-1}).$$

Similar equations govern $\hat{w}$, $\hat{\omega}_3$ and $\hat{T}$:

$$(D^2 - k^2)\hat{w}^{n+1} = \hat{\phi}^{n+1}, \tag{22}$$
$$(D^2 - \lambda^2)\hat{\omega}_3^{n+1} = \hat{f}_\omega^n, \tag{23}$$
$$(D^2 - \mu^2)\hat{T}^{n+1} = \hat{f}_T^n, \tag{24}$$

where

$$\mu^2 = k^2 + \frac{2}{\Delta t},$$
$$\hat{f}_\omega^n = -(D^2 - \lambda^2)\hat{\omega}^n - \frac{4}{\Delta t\sigma}\hat{\omega}^n - \frac{2}{\Delta t\sigma}(a_n\hat{h}_\omega^n + b_n\hat{h}_\omega^{n-1}),$$
$$\hat{f}_T^n = -(D^2 - \mu^2)\hat{T}^n - \frac{4}{\Delta t}\hat{T}^n - \frac{2}{\Delta t}(a_n\hat{h}_T^n + b_n\hat{h}_T^{n-1}).$$

Finally, the horizontal means $\hat{u}(0, 0)$ and $\hat{v}(0, 0)$ must be considered. They satisfy

$$\left(D^2 - \frac{2}{\Delta t\sigma}\right)\hat{u}^{n+1} = \hat{f}_u^n, \tag{25}$$
$$\left(D^2 - \frac{2}{\Delta t\sigma}\right)\hat{v}^{n+1} = \hat{f}_v^n, \tag{26}$$

where, from (16),

$$\hat{f}_{\hat{u}}^n = -\left(D^2 - \frac{2}{\Delta t\sigma}\right)\hat{u}^n - \frac{4}{\Delta t\sigma}\hat{u}^n - \frac{2}{\Delta t\sigma}(a_n\hat{h}_u^n b_n \hat{h}_u^{n-1}),$$
$$\hat{f}_{\hat{v}}^n = -\left(D^2 - \frac{2}{\Delta t\sigma}\right)\hat{v}^n - \frac{4}{\Delta t\sigma}\hat{v}^n - \frac{2}{\Delta t\sigma}(a_n\hat{h}_v^n b_n \hat{h}_v^{n-1}).$$

4. MATHEMATICAL SOLUTION PROCEDURE

The equations to be solved are (21)–(26). Since each is a boundary value problem, there are different possible approaches. Lundbladh *et al.*[1] use the method of superposition, whereby two particular integrals are obtained and then an appropriate linear combination of these two is taken in order to satisfy the boundary conditions. This has the disadvantage that each differential equation must be solved twice. Our solution procedure involves first finding a particular integral of the equation (numerically), then adding appropriate multiples of the complementary functions (which can be obtained analytically) to satisfy the boundary conditions.

For this section we drop the 'hat' and the superscript n or $n+1$. The simplest equation to solve is that for T because we are given explicit boundary conditions for T. We begin by supposing that a particular integral T_{PI} of (24) is known. (The details of how T_{PI} is found will be described later.) The complementary functions of (24) are simply the exponentials $\mathrm{e}^{\mu(z-1/2)}$ and $\mathrm{e}^{-\mu(z+1/2)}$, so the full solution for T must be of the form

$$T = T_{\mathrm{PI}} + T_+\mathrm{e}^{\mu(z-1/2)} + T_-\mathrm{e}^{-\mu(z+1/2)}.$$

The coefficients T_+ and T_- are now chosen so that T satisfies the boundary conditions (10). These coefficients are

$$T_+ = \frac{(-\alpha_{11}\mu + \alpha_{12})\Delta_{\mathrm{top}} - (-\alpha_9\mu + \alpha_{10})\mathrm{e}^{-\mu}\Delta_{\mathrm{btm}}}{(\alpha_9\mu + \alpha_{10})(-\alpha_{11}\mu + \alpha_{12}) - (-\alpha_9\mu + \alpha_{10})(\alpha_{11}\mu + \alpha_{12})\mathrm{e}^{-2\mu}},$$
$$T_- = \frac{-(\alpha_{11}\mu + \alpha_{12})\mathrm{e}^{-\mu}\Delta_{\mathrm{top}} + (\alpha_9\mu + \alpha_{10})\Delta_{\mathrm{btm}}}{(\alpha_9\mu + \alpha_{10})(-\alpha_{11}\mu + \alpha_{12}) - (-\alpha_9\mu + \alpha_{10})(\alpha_{11}\mu + \alpha_{12})\mathrm{e}^{-2\mu}},$$

where

$$\Delta_{\mathrm{top}} = -\alpha_9 T'_{\mathrm{PI}}(\tfrac{1}{2}) - \alpha_{10}T_{\mathrm{PI}}(\tfrac{1}{2}), \qquad \Delta_{\mathrm{btm}} = -\alpha_{11}T'_{\mathrm{PI}}(-\tfrac{1}{2}) - \alpha_{12}T_{\mathrm{PI}}(-\tfrac{1}{2})$$

for modes other than the (0, 0) mode and

$$\Delta_{\mathrm{top}} = -\alpha_9 T'_{\mathrm{PI}}(\tfrac{1}{2}) - \alpha_{10}T_{\mathrm{PI}}(\tfrac{1}{2}) + T_{\mathrm{top}}, \qquad \Delta_{\mathrm{btm}} = -\alpha_{11}T'_{\mathrm{PI}}(-\tfrac{1}{2}) - \alpha_{12}T_{\mathrm{PI}}(-\tfrac{1}{2}) + T_{\mathrm{btm}}$$

for the (0, 0) mode.

The equations for ϕ and ω_3 cannot be solved quite as easily because we do not have boundary conditions for either of these quantities. Our method is first to find particular integrals of the equations for ϕ, w and ω_3, then to calculate corresponding expressions for u and v. In general these expressions do not satisfy the correct boundary conditions, but by adding appropriate complementary functions to ϕ, w and ω_3, this problem can be remedied and the boundary condition for w also can be satisfied. From (21) we have

$$\phi = \phi_{\mathrm{PI}} + \phi_+\mathrm{e}^{\lambda(z-1/2)} + \phi_-\mathrm{e}^{-\lambda(z+1/2)},$$

where ϕ_{PI} is some particular integral and ϕ_+ and ϕ_- are as yet undetermined constants of integration. Equation (22) for w can then be solved to give

$$w = w_{\mathrm{PI}} + w_+ \mathrm{e}^{k(z-1/2)} + w_- \mathrm{e}^{-k(z+1/2)} + \frac{\Delta t \sigma}{2}(\phi_+ \mathrm{e}^{\lambda(z-1/2)} + \phi_- \mathrm{e}^{-\lambda(z+1/2)}),$$

where w_{PI} is some particular integral of $(D^2 - k^2)w_{\mathrm{PI}} = \phi_{\mathrm{PI}}$ and w_+ and w_- are constants of integration. Finally, ω_3 is

$$\omega_3 = \omega_{\mathrm{PI}} + \omega_+ \mathrm{e}^{\lambda(z-1/2)} + \omega_- \mathrm{e}^{-\lambda(z+1/2)}.$$

To construct u and v, we use (15), which becomes

$$u(n_x, n_y) = \frac{\mathrm{i}}{k^2}(n_x k_x Dw + n_y k_y \omega_3), \qquad v(n_x, n_y) = \frac{\mathrm{i}}{k^2}(n_y k_y Dw - n_x k_x \omega_3)$$

for modes other than the (0, 0) mode. Then the six boundary conditions (8) and (9) on u, v and w give six equations to be solved for the six unknowns ϕ_+, ϕ_-, w_+, w_-, ω_+ and ω_-. These are solved systematically in our code.

The horizontal means $\bar{u}$ and $\bar{v}$ are found simply by writing

$$\bar{u} = \bar{u}_{\mathrm{PI}} + \bar{u}_+ \mathrm{e}^{2(z-1/2)/\Delta t\sigma} + \bar{u}_- \mathrm{e}^{-2(z+1/2)/\Delta t\sigma}, \qquad \bar{v} = \bar{v}_{\mathrm{PI}} + \bar{v}_+ \mathrm{e}^{2(z-1/2)/\Delta t\sigma} + \bar{v}_- \mathrm{e}^{-2(z+1/2)/\Delta t\sigma}.$$

Once the particular integrals $\bar{u}_{\mathrm{PI}}$ and $\bar{v}_{\mathrm{PI}}$ are known, the coefficients $\bar{u}_+$, $\bar{u}_-$, $\bar{v}_+$ and $\bar{v}_-$ are determined from the boundary conditions (8) and (9).

5. DISCRETIZATION IN z

We have reduced the problem of time stepping to that of finding a particular integral of ODEs of the form

$$(D^2 - a^2)f(z) = r(z), \tag{27}$$

where a is λ, μ or k. To solve such an equation numerically, we approximate all functions of z by truncated sums of Chebyshev polynomials:[9]

$$f(z) = \sum_{n=0}^{N_z} f_n T_n(Z),$$

where $Z = 2z$.

Following Lundbladh *et al.*,[1] we first calculate f'' and then find f' and f by integration. This procedure is numerically better conditioned than solving directly for f.[10] We suppose that f, f' and f'' are written as the sums

$$f(z) = \sum_0^{N_z} f_n T_n(Z), \qquad f'(z) = \sum_0^{N_z} g_n T_n(Z), \qquad f''(z) = \sum_0^{N_z} h_n T_n(Z). \tag{28}$$

We use the well-known recurrence relation between the Chebyshev coefficients of a function and its derivative:

$$f_n = \frac{1}{4n}(c_{n-1} g_{n-1} - g_{n+1}) \quad \text{for } n = 1, \ldots, N_z, \tag{29}$$

where $c_0 = 2$, $c_n = 1$ for $n > 0$, and $g_{N_z+1} \equiv 0$. This allows us to write (27) as a tridiagonal system of equations for the h_n:

$$h_0 = r_0 + a^2 f_0, \qquad h_1 = r_1 + a^2 f_1,$$

$$\left(1 + \frac{a^2}{24}\right) h_2 - \frac{a^2}{16} h_0 - \frac{a^2}{96} h_4 = r_2,$$

$$\left(1 + \frac{a^2}{8(n^2-1)}\right) h_n - \frac{a^2}{16n(n-1)} h_{n-2} - \frac{a^2}{16n(n+1)} h_{n+2} = r_n, \quad 2 < n < N_z - 1,$$

$$\left(1 + \frac{a^2}{8N_z(N_z-2)}\right) h_{N_z-1} - \frac{a^2}{16(N_z-1)(N_z-2)} h_{N_z-3} = r_{N_z-1},$$

$$\left(1 + \frac{a^2}{16N_z(N_z-1)}\right) h_{N_z} - \frac{a^2}{16N_z(N_z-1)} h_{N_z-2} = r_{N_z}.$$

For any choice of f_0 and f_1 this system will provide the Chebyshev coefficients h_n for the second derivative of some particular integral of (27). The two unknowns f_0 and f_1 correspond to the two constants of integration that can be expected to arise in integrating (27) and we choose for simplicity $f_0 = f_1 = 0$.

The function f itself is then found from a pair of integrations. The first uses the recurrence relation (29) to obtain f' from f''. The coefficient g_0 is undetermined by this step and is set to zero by the numerical integration subroutine, to be corrected later (when we impose the condition $f_1 = 0$). A second use of the recurrence relation gives the coefficients f_n, with f_0 automatically set to zero by the integration subroutine. In general f_1 will not be zero because we have the wrong value of g_0. By subtracting $f_1 T_1(Z)$ from the calculated function f, however, we find the correct solution with $f_0 = f_1 = 0$.

5.1. *Integration correction*

The truncations (28) are, strictly speaking, incompatible. The series (28) for f, f' and f'' are each obtained by imagining these functions to be written as infinite series and then truncating them independently at $n = N_z$. However, if f were truly a sum of the first N_z Chebyshev polynomials, then f' would be a sum of the first $N_z - 1$ and f'' of the first $N_z - 2$. Therefore, if the coefficients f_n were used to reconstruct the coefficients of f', the result would not be the g_n. We have taken no action to correct this, on the grounds that if we take N_z large enough, then such truncation errors will be negligible.

5.2. *Chebyshev polynomials and expansion of complementary functions*

Applying the boundary conditions involves adding combinations of exponential functions to the particular integrals found above, as in Section 4. We therefore need to express an exponential function in terms of Chebyshev polynomials. We use the exact relation

$$\mathrm{e}^{aZ} = I_0(a) + 2 \sum_{n=1}^{\infty} I_n(a) T_n(Z),$$

where I_n is a modified Bessel function. Since the parameters are fixed for the duration of a run and in particular we use a constant time step, the values of λ, μ and k for each Fourier mode do not change in the course of a calculation. We therefore evaluate the coefficients $I_n(a)$ once only, at the start of the calculation.

6. VERIFICATION OF THE CODE

We have checked the code thoroughly against analytical and other numerical results. We began by carrying out fundamental checks on our solutions, for example, using the computer algebra package Maple to reconstruct the temperature and velocity components from their Chebyshev coefficients and verifying that they satisfy the appropriate boundary conditions. We then proceeded to check the results of the code against independent analytical and numerical results. A sample of the checks is described in this section.

6.1. Rayleigh–Bénard convection

A number of checks of the code were carried out using the much-studied problem of Rayleigh–Bénard convection. These are summarized below.

6.1.1. Linear theory. We first checked the growth rates of small disturbances to the basic state. We took as an initial condition for our code a small perturbation from the basic state (i.e. the state of pure heat conduction and no fluid motion). Growth rates were estimated by examining the amplitudes of the Fourier modes.

We compared the calculated growth rates with the eigenvalues of the linear stability problem. For stress-free, fixed temperature boundaries they can be calculated analytically. For other boundary conditions the eigenvalues may be calculated by solving the linear stability problem numerically—see e.g. Reference 3 for details.

Very accurate results were obtained, confirming the spectral accuracy of the code. For example, for stress-free, fixed temperature boundaries with $Ra = 1000$, $L_y = 2$ and $\sigma = 1$ the analytical growth rate is 2·621 and the numerical growth rate at a resolution of $1 \times 6 \times 21$ is 2·620. With rigid, fixed temperature boundaries the minimum critical Rayleigh number is 1708 at $L_y = 2{\cdot}016$.[7] Our code agrees with this result, giving growth rates of $-0{\cdot}013$ at $Ra = 1706$, 0·0018 at $Ra = 1708$ and 0·017 at $Ra = 1710$. These growth rates coincide with those obtained by solving the linear stability problem.

6.1.2. Nonlinear theory. For stress-free, fixed temperature boundaries the weakly non-linear solution can also be obtained analytically, i.e. the amplitude of convection is known for Rayleigh numbers close to critical.[11] The minimum critical Rayleigh number is 657·51 at $L_y = \sqrt{8}$ and weakly non-linear analysis predicts that a two-dimensional solution is stable. At a Rayleigh number of 680 the maximum value of the vertical velocity is predicted to be 2·013 and the Nusselt number 1·0684. Our code gives two-dimensional convection with values of 2·018 and 1·0665 respectively at a resolution of $8 \times 8 \times 21$.

To check our code further from the onset of instability, we compared strongly non-linear results against the work of Moore and Weiss.[12] For stress-free, fixed temperature boundaries with $L_y = \sqrt{8}$ and a Rayleigh number of 3945·07, six times critical, the Nusselt number is 3·585 at a resolution of either $1 \times 16 \times 31$ or $1 \times 32 \times 31$, which agrees with the value 3·58 given by Moore and Weiss.[12]

6.2. Langmuir circulation

Numerical simulations of two-dimensional (x-independent) Langmuir circulation together with weakly non-linear analytical results were described by Cox *et al.*[3] We compared our results with theirs and found excellent agreement. For an unstratified layer ($S_{\mathrm{LT}} = 0$) the agreement between our code and the weakly non-linear prediction of N_+ is given in Table I. The analytical prediction is an asymptotic result, valid in the limit as $N_+ \to 1$ ($R_{\mathrm{LT}} \to R_{\mathrm{LTc}} \approx 458{\cdot}79$). The resolution is $1 \times 12 \times 25$, $\Delta t = 0{\cdot}005$ and $\sigma = 6{\cdot}7$.

Table I. Comparison of our code with weakly non-linear (WNL) results for two-dimensional Langmuir circulation

RLANG (code)	R_{LT}	N_+ (code)	N_+ (WNL)
3140·893	468·79	1·3536	1·424
3107·393	463·79	1·1925	1·212
3087·293	460·79	1·0816	1·0848
3080·593	459·79	1·0417	1·0424
3077·243	459·29	1·0212	1·0212

For $S_{LT} = 80$ we computed a branch of travelling waves at $R_{LT} = 800$ and 1000. At a resolution of $1 \times 16 \times 33$ and with a time step of 0·001, N_+ takes the values 3·265 and 3·849, where Cox *et al.*[3] find 3·264 and 3·848. The difference in each case is less than one part in 1000.

For $S_{LT} = 200$, the bifurcation sequence reported by Cox *et al.*[3] as R_{LT} is increased is that a branch of travelling waves develops a temporal instability to modulated travelling waves, which subsequently cease to exist in a heteroclinic bifurcation to a branch of steady states and standing waves. We found the same sequence of bifurcations at approximately the same parameter values (we are unable to compare precise values because we read bifurcation values from their diagrams).

6.2.1. Long-wavelength Langmuir circulation. To check the implementation of the mixed boundary conditions and the treatment of the linear terms, we compared our results with those of the long-wave theory of Chapman and Proctor[13] and Cox and Leibovich,[8] in which an analytical expression for the linear growth rate of small disturbances is given (see Table II). For Langmuir circulation the physical problem suggests that we set $\alpha_1 = \alpha_3 = \alpha_5 = \alpha_7 = 1$, $\alpha_6 = \frac{1}{2}\alpha_2$ and $\alpha_8 = 0$. The

Table II. Comparison of our code with long-wave results for linear growth rate of small disturbances in two-dimensional Langmuir circulation problem[8]

RLANG/SIGMA (code)	Growth rate (Cox and Leibovich[8])	Growth rate (code)
(i) FF problem: $\alpha_2 = 0{\cdot}01$, $L_y = 10\pi$		
120	−0·010315	−0·01036
130	−0·00698	−0·00706
150	−0·000315	−0·00046
170	0·00635	0·00614
(ii) FR problem: $\alpha_2 = 0{\cdot}01$, $L_y = 10\pi$		
320	−0·010008	−0·010005
330	−0·009696	−0·009694
400	−0·007508	−0·007514
(iii) FR problem: $\alpha_2 = 0{\cdot}01$, $L_y = 20\pi$		
320	−0·010008	−0·009988
330	−0·009696	−0·009677
400	−0·007508	−0·007493
(iv) RR problem: $\alpha_2 = 0{\cdot}01$, $L_y = 10\pi$		
720	−0·01006	−0·01011
730	−0·00950	−0·00955

results of Cox and Leibovich[8] are valid in the limit as $\alpha_2 - \alpha_4 \to 0$ (α_2, $-\alpha_4 > 0$), in which case the horizontal scale of the motion is very large compared with the layer depth (which is non-dimensionalized to unity). For validity of the analytical results we must also have R_{LT} close to R_{LTc}, where R_{LTc} is given below. The resolution of the numerical runs was $1 \times 12 \times 25$ and $\Delta t = 0{\cdot}002$. We took the special case in which $\alpha_4 = 0$ and considered the four separate problems listed below. Only the first and second are physically reasonable models for Langmuir circulation, but there is a mathematical analogy between two-dimensional Langmuir circulation and Rayleigh–Bénard convection and so the third and fourth cases also have physically meaningful interpretations. The problems are: (i) both horizontal boundaries stress-free (FF, $R_{LTc} \approx 120$); (ii) the upper boundary stress-free and the lower rigid (FR, $R_{LTc} \approx 320$); (iii) the upper boundary rigid and the lower stress-free (RF, $R_{LTc} \approx 320$); (iv) both horizontal boundaries rigid (RR, $R_{LTc} \approx 720$).

7. CONVECTION IN SHEAR FLOW

In this section we describe four simulations of convection at large Rayleigh number which indicate the effects of a strong shear flow. We originally intended these calculations to be a further check on our code by comparing our results with corresponding results of Hathaway and Somerville.[4] However, we found a wider variety of behaviour than that reported by Hathaway and Somerville,[4] most likely because they terminated their integrations after 1·3 dimensionless time units (or less) whereas we continued ours for about 10 times as long. They described how the fluid reached a state of 'quasi-equilibrium' by $t = 1{\cdot}3$. We found that significant development of the pattern occurs well after this time and also that different stable solutions can be obtained depending on the initial conditions.

We took isothermal, rigid boundaries with an applied shear in the x-direction. Thus $\alpha_j = 0$ for odd j and $\alpha_j = 1$ for even j. Also $U_{top} = \frac{1}{2}U_{shear}$, $U_{btm} = -\frac{1}{2}U_{shear}$, $V_{top} = V_{btm} = 0$, $T_{top} = 0$ and $T_{btm} = 1$. The basic state shear was then simply U_{shear}. Following Hathaway and Somerville,[4] we investigated four values of U_{shear} ($= 0$, 50, 100, 200) and took a unit Prandtl number. The computational domain was $0 \leqslant x, y \leqslant 10$ (the depth of the fluid layer being normalized to unity). The Rayleigh number was fixed at $Ra = 10{,}000$ for all runs, which is about six times the critical Rayleigh number for convection with rigid boundaries. For all our integrations the spatial resolution was $N_x = N_y = 48$ and $N_z = 41$. Our initial condition was the equilibrium state plus a small, random perturbation to each Fourier mode, except where stated otherwise below.

In the absence of shear ($U_{shear} = 0$) the convection was three-dimensional, disordered and unsteady. Figure 1 shows a typical convection pattern in the (x, y) plane viewed from above. The figure shows an iso-surface of the vertical velocity component w towards the end of the computation. The iso-surface value is $w = 2$, and the maximum vertical velocity is about 30. The computation was continued until $t = 30$ to ensure that the system did not settle down to any regular behaviour. Recall that these are diffusive time units: $t = 30$ corresponds to over 100 turnover times. The Nusselt number fluctuated between 2·1 and 2·3. To check whether the flow was chaotic, the final 10 time units of the computation were repeated with a small perturbation ($\pm 1\%$) added to the velocity and temperature fields. This showed exponential divergence from the first run, indicating that the flow was indeed chaotic with a Lyapunov exponent of about 1·8.

The convection in the presence of a shear flow with $U_{shear} = 50$ became aligned with the direction of shear and took the form of three pairs of wavy rolls as shown in Figure 2. The pattern travelled in the direction of increasing x with a phase speed (dx/dt) of approximately 16·0. The Nusselt number was 2·36. This right-travelling solution enables us to infer the existence of a corresponding solution travelling to the left because of the symmetry of the governing equations and boundary conditions. Our Nusselt number is consistent with the value 2·34 found by Hathaway and Somerville[4] after 1·3 time units.

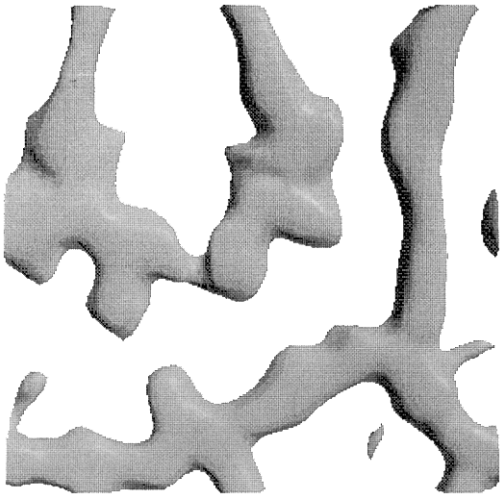

Figure 1. Iso-surface of vertical velocity for convection at $U_{\text{shear}} = 0$

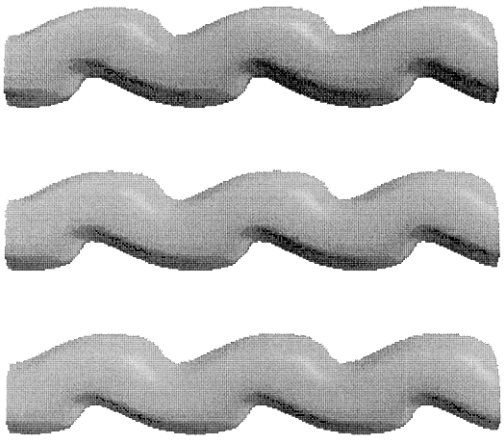

Figure 2. Planform of convection for $U_{\text{shear}} = 50$. The pattern drifts to the right. We infer the existence of a mirror-image left-travelling pattern

For stronger shear ($U_{\text{shear}} = 100$), the convection was organized into five pairs of parallel rolls aligned with the shear, with no waviness of the rolls apparent (see Figure 3). The Nusselt number was 2·615. By contrast, Hathaway and Somerville[4] found three pairs of rolls with a Nusselt number of 2·37. To resolve the discrepancy, we performed a second run at the same parameter values but with a different initial condition. This time, in addition to the random choice of Fourier coefficients, we added a strong component of the (0, 3) mode. After approximately 15 time units a stationary pattern of three pairs of wavy rolls developed as in Figure 4. The Nusselt number was 2·345. We checked that both solutions were stable by examining the growth or decay of Fourier modes: all the mode amplitudes were either stationary or decaying. It seems, therefore, that the patterns of five straight

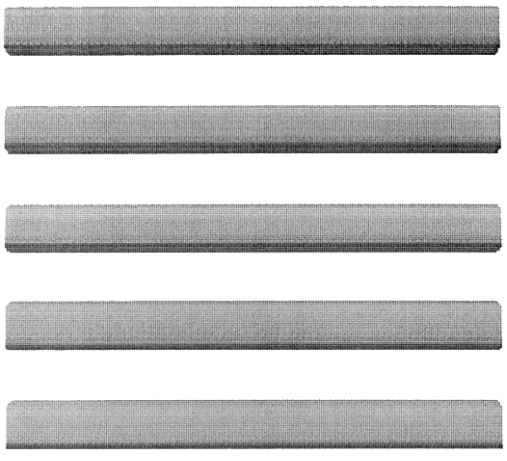

Figure 3. A stable planform of convection for $U_{\text{shear}} = 100$

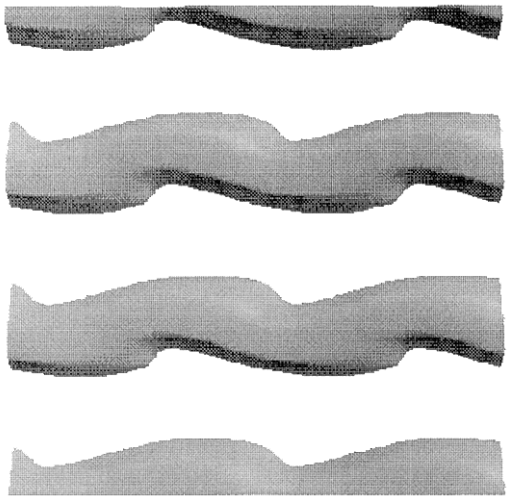

Figure 4. Another stable planform of convection for $U_{\text{shear}} = 100$

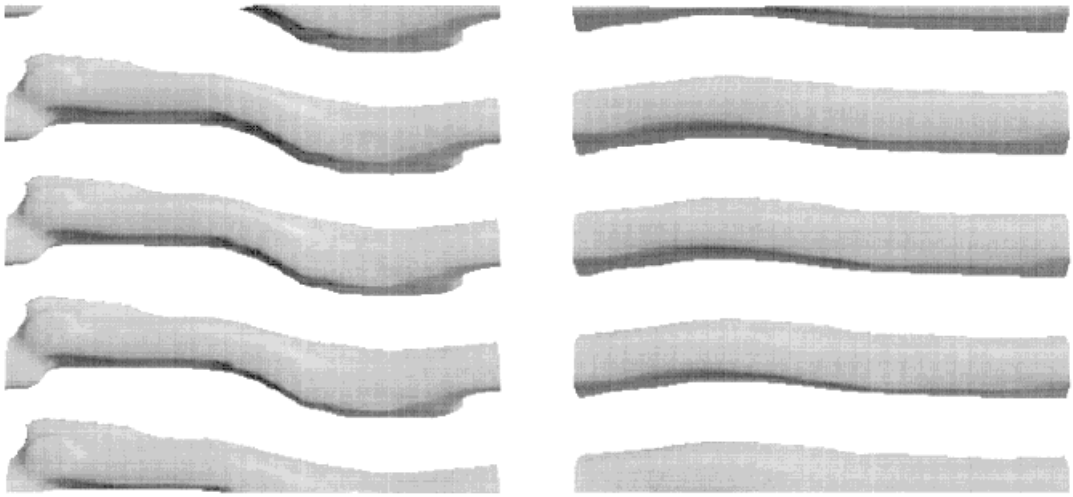

Figure 5. Planform of convection for $U_{\text{shear}} = 200$ at two stages of recurrent sequence of bursts. (a) Towards the start of a burst, the rolls develop significant waviness. (b) Later in the burst, as the burst subsides, the rolls become almost two-dimensional, and remain so during the quiescent period

rolls and three wavy rolls were both stable and were selected according to the initial conditions used. Note that there are fewer waves along the rolls in Figure 4 than in Figure 2, which corresponds to weaker shear. Thus for stronger shear the three pairs of rolls are more closely aligned with the direction of shear. A stable pattern with four pairs of rolls was also found by starting from the random initial condition plus a (0, 4) mode component.

A new phenomenon occurred when the shear was increased further. The solution for $U_{\text{shear}} = 200$ consisted of four pairs of strongly time-dependent wavy rolls (see Figure 5). These rolls exhibited a recurrent sequence of 'bursting' events during which the convection was strongly three-dimensional, separated by quiescent periods where the convection was organized into slightly wavy rolls. The bursts lasted approximately 1 time unit and the separation between bursts was approximately 4 time units. Figure 5(a) shows the rolls at the start of a burst. As the burst progressed, the marked three-dimensionality of the rolls declined: Figure 5(b) shows a typical solution near the beginning of the quiescent period. The interval between the two plots is 1 time unit. For comparison, Hathaway and Somerville[4] reported a final state of straight rolls at $t = 0{\cdot}65$; since the period of the bursting events is approximately 4 time units, it seems that their integrations were of insufficient length to find any signs of bursting.

8. CONCLUSIONS

We have described a code for simulating three-dimensional convection in a layer of incompressible, Newtonian fluid. The mechanism driving the convection may be of thermal or mechanical origin and the fluid layer may be rotating. A novel feature of the code is its manner of implementing the conditions to be applied to the temperature and velocity fields at the horizontal boundaries. This enables mixed boundary conditions to be applied with a single integration step coupled to a numerical/analytical modification of the integrated solution to fit the boundary conditions, rather than a pair of integrations followed by a superposition. We have described some of the comprehensive list

of checks to which we have subjected the code and we believe these offer firm evidence of the code's accuracy.

By extending the calculations of Hathaway and Somerville,[4] we have discovered a richer set of solutions than suggested by their short-time integrations. Many questions remain to be answered, however, for example, the route by which the chaos arises in the unsheared case and how the distinct upstream and downstream travelling patterns of wavy rolls arise in the case of $U_{\text{shear}} = 50$.

ACKNOWLEDGEMENTS

We wish to acknowledge financial support from the Nuffield Foundation (through Newly Appointed Science Lecturers awards to S.M.C. and P.C.M.), the University of Nottingham (through a New Lecturers Research Grant to S.M.C. and P.C.M.) and the Royal Society (P.C.M.).

We are grateful to Dan Henningson for providing us with the transform subroutines.

All figures were produced with the visualization package SciAn.

REFERENCES

1. A. Lundbladh, D. S. Henningson and A. V. Johansson, 'An efficient spectral integration method for the solution of the Navier–Stokes equations', *Rep. FFA-TN 1992-28*, Aeronautical Research Institute of Sweden, 1992.
2. A. D. D. Craik and S. Leibovich, 'A rational model for Langmuir circulations', *J. Fluid Mech.*, **73**, 401–426 (1976).
3. S. M. Cox, S. Leibovich, I. M. Moroz and A. Tandon, 'Nonlinear dynamics in Langmuir circulations with O(2) symmetry', *J. Fluid Mech.*, **241**, 669–704 (1992).
4. D. H. Hathaway and R. C. Somerville, 'Nonlinear interactions between convection, rotation and flows with vertical shear', *J. Fluid Mech.*, **164**, 91–105 (1986).
5. P. G. Drazin and W. H. Reid, *Hydrodynamic Stability*, Cambridge University Press, Cambridge, 1981.
6. A. Tandon and S. Leibovich, 'Three-dimensional Langmuir circulation instability in a stratified layer', *J. Geophys. Res.*, **98**, 16,501–16,507 (1993).
7. S. Chandrasekhar, *Hydrodynamic and Hydromagnetic Stability*, Oxford University Press, Oxford, 1961.
8. S. M. Cox and S. Leibovich, 'Langmuir circulations in a surface layer bounded by a strong thermocline', *J. Phys. Oceanogr.*, **23**, 1330–1345 (1993).
9. D. Gottlieb and S. A. Orszag, *Numerical Analysis of Spectral Methods: Theory and Applications*, SIAM, Philadelphia, PA, 1977.
10. L. Greengard, 'Spectral integration and two-point boundary value problems', *SIAM J. Numer. Anal.*, **28**, 1071–1080 (1991).
11. W. V. R. Malkus and G. Veronis, 'Finite amplitude cellular convection', *J. Fluid Mech.*, **4**, 225–260 (1958).
12. D. R. Moore and N. O. Weiss, 'Nonlinear penetrative convection', *J. Fluid Mech*., **61**, 553–581 (1973).
13. C. J. Chapman and M. R. E. Proctor, 'Nonlinear Rayleigh–Bénard convection between poorly conducting boundaries', *J. Fluid Mech.*, **101**, 759–782 (1980).

